

### Key Points:

- Robust long-term cooling trends exist between 100 and 200 m in the Pacific off-equatorial region in historical and SSP2-4.5 simulation
- Spiciness variation and thermocline heave are both important in driving the off-equatorial subsurface cooling at a fixed level
- The maximum cooling spiciness trends occur in the eastern subtropics, mainly due to direct subduction and anomalous advection processes

### Supporting Information:

Supporting Information may be found in the online version of this article.

### Correspondence to:

Y. Du,  
duyan@scsio.ac.cn

### Citation:

Ju, W.-S., Zhang, Y., & Du, Y. (2022). Subsurface cooling in the tropical Pacific under a warming climate. *Journal of Geophysical Research: Oceans*, 127, e2021JC018225. <https://doi.org/10.1029/2021JC018225>

Received 8 NOV 2021

Accepted 28 APR 2022

## Subsurface Cooling in the Tropical Pacific Under a Warming Climate

Wen-Shan Ju<sup>1,2,3</sup>, Ying Zhang<sup>1,3</sup>, and Yan Du<sup>1,2,3</sup> 

<sup>1</sup>State Key Laboratory of Tropical Oceanography, South China Sea Institute of Oceanology, Chinese Academy of Sciences, Guangzhou, China, <sup>2</sup>University of Chinese Academy of Sciences, Beijing, China, <sup>3</sup>Southern Marine Science and Engineering Guangdong Laboratory (Guangzhou), Guangzhou, China

**Abstract** The present study investigates the subsurface temperature trend in the tropical Pacific in historical and SSP2-4.5 simulation by 14 models from Coupled Model Intercomparison Project Phase 6. Robust cooling trends exist between 100 and 200 m in the off-equatorial region ( $2^{\circ}$ – $8^{\circ}$ N/S) of both the North and South Pacific during 1950–2100. Both spiciness variation and thermocline heave are important in driving this off-equatorial subsurface cooling at a fixed level. The cooling spiciness trends in the off-equatorial region originates from the eastern subtropical Pacific along isopycnal streamlines. Besides, the contribution of the thermocline heave to the cooling is governed by the large wind stress curl trend. Furthermore, the maximum negative spiciness trends occur in the eastern subtropics of both the North and South Pacific. The consistently poleward migration of outcropping lines makes cooler subducting water at higher latitudes directly flow into the subtropical subsurface, which induces the negative spiciness trends here. The generation of the negative spiciness trends is also partly attributed to the anomalous advection process on distinct isopycnal surfaces. These two processes both contribute to the generation of spiciness variation in both the North and South Pacific. The generation region is partly covered by the outcropping region, thus, the strong vertical mixing within the mixed layer may weaken the effect of the subduction and advection. This study mainly highlights the significance of the spiciness variation in the projection of the subsurface temperature trend on a longer time scale under global warming.

**Plain Language Summary** Temperature change in the tropical Pacific has crucial impacts on changes in regional or global climate variables, such as precipitation, large-scale circulation, and even climate feedback. Besides the sea surface temperature that most studies focus on, the subsurface temperature can affect the upper ocean thermal structure, which further modulates the air-sea interactions through vertical processes, so it is also vital to investigate the subsurface temperature change in a warming climate. In this study, we find two robust symmetric subsurface cooling trends in the tropical Pacific off-equatorial region and elucidate two important impact factors of these cooling trends: spiciness variation and thermocline heave. The former is the temperature/salinity anomaly along the isopycnal surface, and the latter is the vertical displacement of the mean thermocline. Negative spiciness trends originated from the eastern subtropics and local thermocline shallowing induce the subsurface cooling in the off-equatorial Pacific. We also find that both the direct subduction and anomalous advection processes can induce the maximum cooling trends in the eastern subtropics. The present study shows that spiciness variation is the same significance as thermocline heave, while most previous studies neglect the former's contribution.

## 1. Introduction

Due to the increase of greenhouse gas (GHG) concentrations coupled with the long response timescales and large thermal capacity of the oceans, a large amount of the global warming heat entering Earth's climate system is taken to the ocean and mainly stored in the upper ocean layer (Johnson & Lyman, 2020; Levitus et al., 2005, 2012). Ocean temperature change is the main metric of ocean warming linked to the increasing GHG concentrations. Temperature change in the tropical region is one of the most important issues, which has crucial impacts on changes in some other regional or global climate variables, such as precipitation, large-scale circulation (Ma & Xie, 2013; Shin & Sardeshmukh, 2011; Tokinaga et al., 2012; Xie et al., 2010), and even climate feedback (Andrews & Webb, 2018). The subsurface temperature is a principal part of the upper ocean layers. Its change can affect the upper ocean thermal structure, modulating the air-sea coupling processes over the tropical region (Kakatkar et al., 2020). Furthermore, several previous studies have indicated the significant role of

subsurface ocean temperature in predicting the atmospheric variables (tropical cyclone, air temperature, etc.) on seasonal, interannual and decadal timescales (Bratcher & Giese, 2002; Schneider et al., 1999a, 1999b; Sparks & Toumi, 2020). As a result, with the increasing GHG concentrations, a better understanding of the long-term tropical subsurface temperature trend is of great scientific value.

The global ocean heat content has been proven to increase until at least 2,300 for all plausible scenarios (Bindoff, 2019; Palmer et al., 2018). However, several previous studies indicated the subsurface cooling in the tropical Pacific Ocean based on coupled climate models with different increasing CO<sub>2</sub> experiments (Du & Xie, 2008; Luo et al., 2011, 2018). This subsurface cooling in the warming ocean draws attention. Yang (2009) showed weaker warming along the equatorial thermocline than at the surface in transient and equilibrium CO<sub>2</sub> experiments and pointed out that the slowdown of the Subtropical Cells (STCs) is an important factor in cooling the subsurface temperature in the western equatorial Pacific. Luo (2018) showed a cooling signal along with the Pacific western equatorial thermocline response to CO<sub>2</sub> quadrupling and suggested that a combination of the weakened equatorial easterlies and direct radiative forcing emission sets the subsurface temperature structure at the equator. Luo (2011, 2018) also found that the maximum of the relative subsurface cooling appears to be around 5° latitude and suggested that the upwelling and thermocline shoaling induced by wind stress change are the keys to determining this off-equatorial cooling. However, studies about such tropical Pacific subsurface cooling are limited, and the mechanisms are still unclear. Thus, based on the new CMIP6 multimodel ensemble, the long-term subsurface temperature trends in the tropical Pacific and related mechanisms will be explored in detail in this study.

Above all, thermocline heaving is the primal process that causes the temperature variability at a fixed level in the ocean interior, and another impact factor is spiciness variation (Arbic & Owens, 2001; Bindoff & McDougall, 1994; Nagura et al., 2018). Thermocline heaving is the vertical displacement of the mean thermocline accompanied by vertical density structure change, caused by either adiabatic processes (wind forcing changes) or diabatic heat flux divergence (Häkkinen et al., 2016). On multidecadal time scale, horizontal advection is the main cause for heaving, while low-frequency ocean dynamics, such as strengthening changes of the gyre, could also contribute (Church et al., 1991; Häkkinen et al., 2016). The spiciness has been defined by Munk (1981) as density compensated anomalies of temperature and salinity and does therefore not affect the density profile. Spiciness anomalies can be produced in the outcropping region through air-sea interaction and anomalous subduction (Johnson, 2006). Outside the outcropping region, anomalies can also be generated by convective mixing and isopycnal advection across spiciness fronts (Kolodziejczyk & Gaillard, 2013; Li & Wang, 2015; Schneider, 2000; Wang & Luo, 2020; Yeager & Large, 2004). On decadal/multidecadal timescale, extratropical spiciness anomalies can migrate to the tropics by wind-driven ocean circulation and affect the tropical climate variability (Gu & Philander, 1997; McCreary & Lu, 1994).

This study examines the low-frequency heaving and spiciness variations in the North and South Pacific and their impact on the tropical subsurface Pacific based on the CMIP6. This paper is structured as follows: Section 2 introduces the data and method we use. Section 3 briefly shows the CMIP6 models' performance and summarizes the off-equatorial subsurface cooling in the Pacific. Section 4 investigates the mechanisms of such cooling, introducing the propagation and generation of spiciness anomalies as well as the heaving process. Section 5 provides the conclusion and discussion.

## 2. Data and Method

### 2.1. CMIP6

Historical (1950–2014) and the Share Socioeconomic Pathway 2–4.5 (SSP2-4.5) simulations (2015–2100) from the CMIP6 archive (Eyring et al., 2016) are used in the present study. Fourteen climate models are included to obtain the ensemble trends based on historical and SSP2-4.5 simulations (BCC-CSM2-MR, CESM2-WACCM, CIESM, CNRM-CM6-1, CNRM-ESM2-1, CanESM5, EC-Earth3-Veg, EC-Earth3, FGOALS-f3-L, FIO-ESM-2-0, INM-CM4-8, IPSL-CM6A-LR, MIROC6, UKESM1-0-LL). The models contain the direct outputs of the variables (temperature, salinity, velocity, etc.) we need and can simulate their climatological patterns well. Only one-number run (r1i1p1) from each model, with all variables, be interpolated onto a common grid of 1° × 1°, is used. Furthermore, to remove the high-frequency signal from the long-term trend from 1950 to 2100, we perform 11-year low-pass filtering on time series.

## 2.2. Objective Analysis and Reanalysis Data

Part of the historical and future scenario's simulations are compared against Argo observations to evaluate the model's performance of mean vertical pattern. We use available temperature and salinity global-gridded data of Roemmich-Gilson (RG) Argo Climatology from January 2004 to December 2020. The RG Argo Climatology uses a weighted least squares fit to get the nearest 100 Argo profiles within a given month to estimate the mean field (Roemmich & Gilson, 2009).

Two objective analysis products (EN4, Ishii data set) and one reanalysis product (the Institute of Atmospheric Physics ocean gridded product, IAP) are also used to confirm the accuracy of the temperature trend in CMIP6 models. EN4.2.1 is the UK Met Office Hadley Centre's subsurface temperature and salinity data set, spanning 1900 to present at a monthly timestep. The analysis files have  $1^\circ$  by  $1^\circ$  horizontal resolution and 42 irregularly spaced depth levels for  $83^\circ\text{S}$  to  $90^\circ\text{N}$  (Good et al., 2013). IAP data set feature global coverage of the oceans, at  $1^\circ \times 1^\circ$  horizontal resolution on 41 vertical levels from 1 to 2,000 m, and monthly resolution from 1940 to present (Cheng & Zhu, 2016). The Ishii data are monthly objectively analyzed subsurface temperatures and salinities at 24 levels in the upper 1500 m started from 1945 to 2012 with a horizontal resolution of  $1^\circ \times 1^\circ$  (Ishii et al., 2005). The present study uses the EN4 and IAP temperature field from 1950 to 2020 and Ishii data from 1945 to 2012 to compare with the outputs from CMIP6.

## 2.3. Method

Temporal variability in the temperature at a fixed pressure can be decomposed into contributions from spiciness variation and thermocline heave (Arbic & Owens, 2001). In order to estimate the generation and propagation mechanisms of the subsurface temperature trend, we calculate these two components:

$$\frac{d\theta}{dt} \Big|_p = \frac{d\theta}{dt} \Big|_n - \frac{dp}{dt} \Big|_n \frac{\partial\theta}{\partial p} \quad (1)$$

where  $\theta$  and  $p$  denote potential temperature and pressure. The subscripts  $p$  and  $n$  denote the isobaric surface and the isopycnal surface, respectively. The first term on the right-hand side (RHS) represents temperature variability owing to spiciness variation and is referred to as the spiciness term here. The second term of the RHS is due to thermocline heave, referred to as the heave term (Nagura & Kouketsu, 2018). We calculate  $d\theta/dt|_n$  and  $dp/dt|_n$  as the long-term (1950–2100) trend of isopycnal temperature and pressure. The vertical gradients of temperature ( $\partial\theta/\partial p$ ) are calculated as the mean from 1950 to 2100.

To examine the long-term trend of tropical Pacific zonal currents in more detail, we evaluate their transport changes (Chen et al., 2016), which are defined by:

$$T(x, t) = \int_s^N \bar{u}(x, y, t) dy \quad (2)$$

where  $N(S)$  represents the northernmost (southernmost) latitude of the surface zonal currents,  $\bar{u}(x, y, t)$  is the zonal velocity integrated into the upper ocean 0–300 m, and  $y$  is the latitudinal position of the zonal velocity. It is set to be zero if it is eastward when investigating North Equatorial Current (NEC) and westward when investigating North Equatorial Countercurrent (NECC).

We also use the decompositions to quantify the oceanic horizontal advection at a distinct isopycnal surface:

$$Q_x = -u' \overline{T}_x - \bar{u} T'_x - u' T'_x \quad (3)$$

$$Q_y = -v' \overline{T}_y - \bar{v} T'_y - v' T'_y \quad (4)$$

where  $Q_x$  and  $Q_y$  are the zonal and meridional advection;  $u$  and  $v$  are the zonal and meridional velocity;  $T_x$  and  $T_y$  are the temperature gradients in zonal and meridional directions, respectively. The overbar and prime represent the climatological mean and change from the first 20-year mean (1951–1970). The three terms on the RHS of Equations 3 and 4 indicate the contributions from ocean current changes, temperature gradient changes, and nonlinear terms, respectively (Luo et al., 2018; Yang et al., 2009).

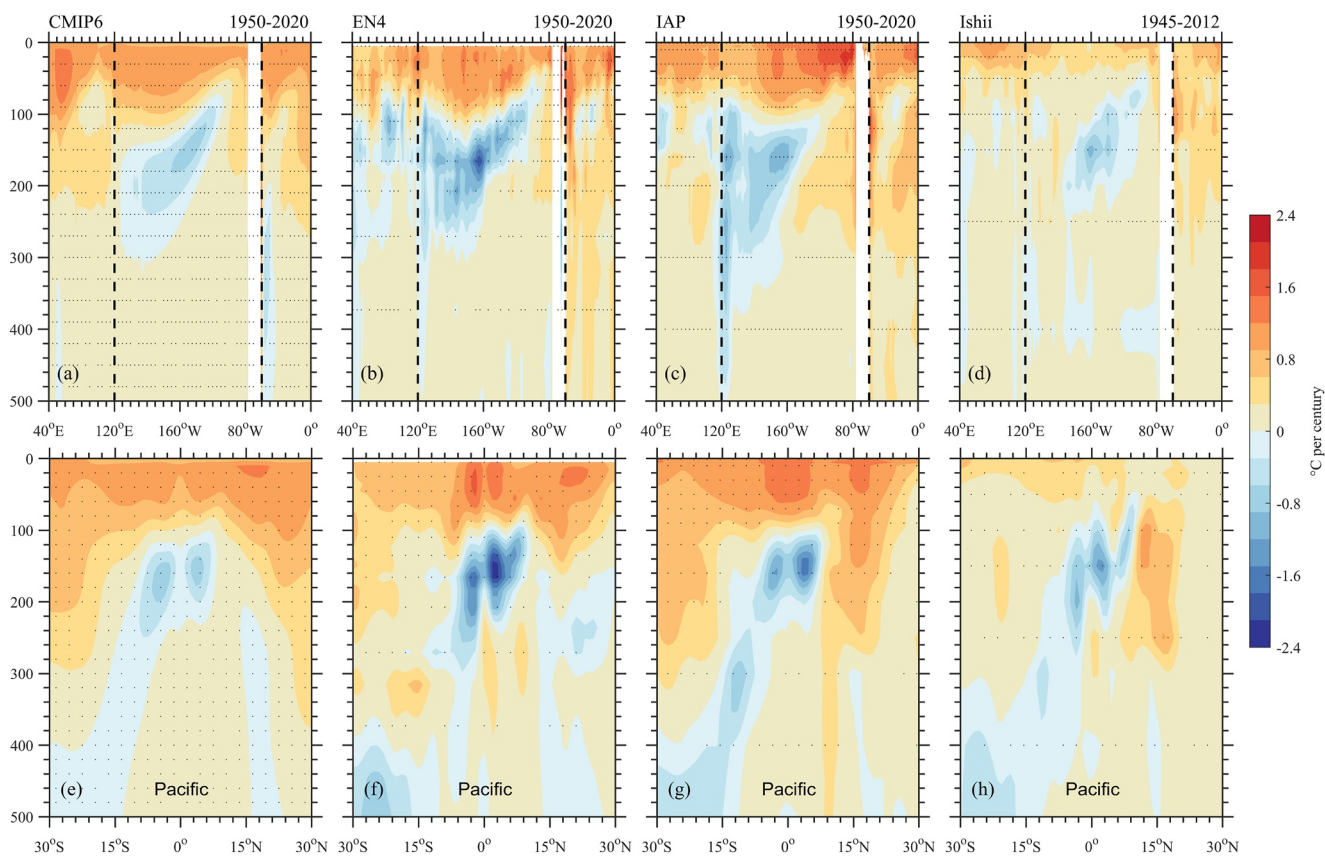


**Figure 1.** (a–d) Meridional mean ( $10^{\circ}\text{S}$ – $10^{\circ}\text{N}$ ) and (e–h) zonal mean ( $160^{\circ}\text{E}$ – $120^{\circ}\text{W}$ ) temperature trend (shading,  $^{\circ}\text{C}$  per century). The results are from (a, e) Coupled Model Intercomparison Project Phase 6 (CMIP6) multimodel ensemble mean; (b, f) EN4 data set; (c, g) IAP product; and (d, h) Ishii data. Note. The trends are calculated from 1945 to 2012 in Ishii data while from 1950 to 2020 in others. The dash lines in (a–d) indicate the longitudes that separate the three basins ( $120^{\circ}\text{E}$ ,  $60^{\circ}\text{W}$ ). Stippling indicates regions where the trends pass the 95% confidence level (Student's *t* test).

### 3. Subsurface Temperature Anomalies

Above all, the multimodel ensemble mean (MME) of temperature trend from 1950 to 2020 in the tropical region over three ocean basins indicates a cooling trend mainly in the subsurface Pacific around 50–300 m (Figure 1a), which shows consensus with the result in CMIP3 (Du & Xie, 2008). When it comes to the details, the core of the subsurface cooling trend locates in both the north and south off-equatorial region of the interior tropical Pacific (Figure 1e). Furthermore, observational data sets, EN4, IAP, and Ishii, are used to evaluate the authenticity of this subsurface cooling trend in CMIP6 models. All observations show general warming above 100 m while subsurface off-equatorial cooling in the tropical Pacific, providing strong evidence for this cooling trend. The result from Ishii data is slightly different from the others, with a small cooling range in the meridional mean. All the three analysis data sets use the same raw data from World Ocean Data set (Boyer et al., 2013), so the difference in the Ishii data set may be due to the uncertainty in the quality-control processes, mapping methods, and XBT/MBT correction (Wang et al., 2018). The temperature trend pattern in CMIP6 is consistent with that in observations (Figure 1). The magnitude of the trend is generally smaller in CMIP6 than in observations, which is largely due to the averaging over the models.

It is also of great significance to investigate the tropical Pacific temperature trend under the scenario of increasing GHG emission (SSP2-4.5). Hence, the present study pays more attention to the temperature trend until the end of the 21st century. Climate models exhibit considerable differences in their simulations of present-day mean states and are subject to various biases relative to available observations (Flato et al., 2013). The observations are not meant to be a strict reference but to serve as a guide to facilitate model intercomparison (McKenna et al., 2020). Besides, the model mean-state biases might provide some context for explaining uncertainty in future climate projections (Lyu et al., 2020). To understand the long-term subsurface temperature trend in the

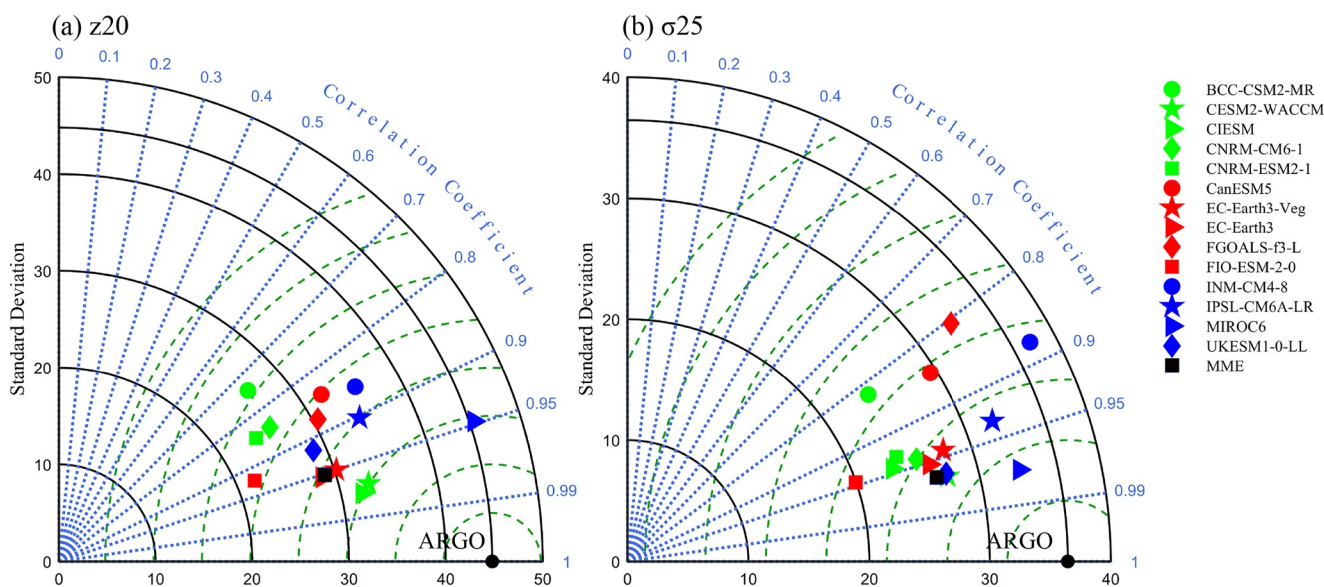


**Figure 2.** Taylor diagrams showing the statistics of (a) the 20 °C isotherm depth and (b) the  $\sigma_{25.0}$  isopycnal depth between the 14 Coupled Model Intercomparison Project Phase 6 (CMIP6) models and Argo buoy derived data (black dot). Black square indicates multimodel ensemble mean. The spatial correlation coefficient  $R$ , standard deviation (STD) (m), and centered RMS (m) are carried out. Green contour represents root-mean-square differences (RMSDs) with an interval of 5 m. Mean spatial patterns are calculated between 10°S and 10°N and 160°E–120°W of the Pacific Ocean and averaged from 2004 to 2020 in each model and Argo data.

tropical Pacific based on CMIP6 models, we use Argo observations to evaluate the CMIP6 models' performance in simulating mean spatial patterns of 20°C isotherm depth ( $z_{20}$ , thermocline depth) and  $\sigma = 25.0 \text{ kg} \cdot \text{m}^{-3}$  ( $\sigma_{25.0}$ ) isopycnal depth. The CMIP6 models can simulate the tropical Pacific vertical structure reasonably well, with the spatial correlations between the simulations and observations generally above 0.7 (Figure 2). The MME shows a great simulation with spatial correlations above 0.95 (Figure 2). The root-mean-square differences (RMSDs) and standard deviations (STD) of  $z_{20}$  are slightly larger than those on  $\sigma_{25.0}$ . The spatial and time average of the depth of  $z_{20}$  ( $\sigma_{25.0}$ ) is approximately 147 (145) m in Argo data and 134 (147) m in MME.

When it comes to the long-term temperature trend from 1950 to 2100, the MME result also indicates a subsurface cooling in the tropical Pacific, but with a smaller extent at 100–250 m than from 1950 to 2020 (Figures 1a and 3a). Furthermore, only two models (CanESM5, IPSL-CM6A-LR) show an obvious cooling trend around 300–500 m in the tropical Indian Ocean (Figure S1 in Supporting Information S1). However, it is much smaller than that in the subsurface Pacific in the MME and is therefore ignored in this study. There is a weak subsurface warming trend in the equator and subsurface cooling trend in both the north and south off-equatorial region in the interior tropical Pacific from 1950 to 2100, compared with the subsurface cooling trend through the entire tropical region before 2020 (Figures 1e and 3b). This off-equatorial subsurface cooling trend is robust in the CMIP6 models, despite weak cooling signal in some models (Figure S2 in Supporting Information S1). The magnitude and extent of cooling in the Northern and Southern hemispheres are not completely the same in each model, such as stronger cooling in the north (CIESM, CanESM5, IPSL-CM6A-LR) or more widespread in the south (CESM2-WACCM, CNRM-ESM2-1, FGOALS-f3-L; Figure S2 in Supporting Information S1). Nevertheless, the present study focuses on the MME result and almost neglects the magnitude difference of cooling signal between the Northern and Southern hemispheres. Different from the enhanced warming in the surface layer under the global warming scenario, the cooling in the subsurface layer needs to be explained in detail.

For further analysis, we transform the isobaric coordinates to the isopycnic coordinates. The zonally averaged temperature trend in the Pacific shows that the off-equatorial subsurface cooling trend locates between 2° and 8°N (S) horizontally and  $\sigma_{23.5}$ – $\sigma_{26.0}$  vertically with a magnitude of approximately  $-0.3$  °C per century in the Northern hemisphere as well as  $-0.25$  °C per century in the Southern hemisphere (Figure 4d). As a result, the present study defines the off-equatorial subsurface region (hereafter, OES region) as the region over 2°–8°N (S) and  $\sigma_{23.5}$ – $\sigma_{26.0}$ . According to Equation 1, the contributions of the spiciness process and heaving process to the cooling signal are quantified, respectively. The spiciness term has a large amplitude from 20° to 40°N (S) with

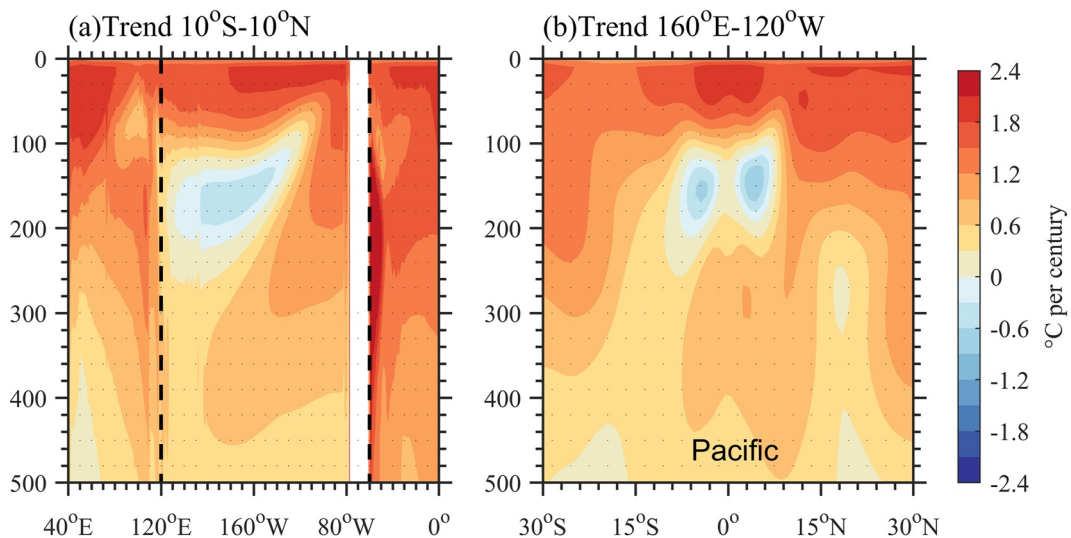


**Figure 3.** (a) Meridional mean ( $10^{\circ}\text{S}$ – $10^{\circ}\text{N}$ ) and (b) zonal mean ( $160^{\circ}\text{E}$ – $120^{\circ}\text{W}$ ) temperature trends (shading,  $^{\circ}\text{C}$  per century) from 1950 to 2100 in the Coupled Model Intercomparison Project Phase 6 (CMIP6) multimodel ensemble mean. The dash lines indicate the longitudes that separate the three basins ( $120^{\circ}\text{E}$ ,  $60^{\circ}\text{W}$ ). Stippling indicates regions where the trends pass the 95% confidence level (Student's *t* test).

two cooling peaks at around  $\sigma 25.0$  in  $25^{\circ}\text{N}$  and around  $\sigma 26.2$  in  $30^{\circ}\text{S}$  (Figure 4a). The heaving term has similar peaks with the spiciness term in the midlatitude region. However, they have the opposite contributions to the isobaric temperature variability (Figures 4a and 4b). Thus, they largely offset each other and eventually positively contribute to the subtropical subsurface ocean. Significantly, these two processes have a cooling contribution in the OES region. Considering a smaller region of cooling induced by the heaving process (Figure 4b), the contributions of two processes are calculated between  $3^{\circ}\text{N}$  and  $7^{\circ}\text{N}$  (S) and  $\sigma 24$ – $\sigma 26$ , which is contained in the OES region. In terms of the spatial average of the region, the magnitude of the spiciness trend is  $-0.25$  ( $-0.13$ )  $^{\circ}\text{C}$  per century and the heaving trend is  $-0.18$  ( $-0.22$ )  $^{\circ}\text{C}$  per century in the north (south). It demonstrates that the contribution of spiciness variation is also as important as thermocline heave, especially in the Northern hemisphere, rather than the dominant role of the thermocline heave proposed in previous studies. The total contribution of the two processes in Figure 4c shows a similar structure with temperature trends directly calculated from model temperature data (Figure 4d), emphasizing the importance of the two processes. The following section will explain in detail why spiciness and heaving processes have negative contributions to the OES region.

## 4. Mechanisms

### 4.1. Spiciness Propagation

The tropical region can be connected to the subtropical region through STCs in the Pacific. Temperature anomalies in midlatitudes can be advected to the tropics with the mean STCs circulation, playing a primary role in equatorial decadal variability (Gu & Philander, 1997; Nonaka et al., 2002). Furthermore, changes in the STCs strength may also modulate the tropical Pacific climate by affecting the equatorial upwelling rate (Kleeman et al., 1999). Zeller et al. (2019) also indicate that the North Hemisphere (NH) STC appears to lead the South Hemisphere (SH) STC by 3 months during El Niño and La Niña events, especially the NH surface branch, so the NH surface transport is also the main factor affecting the mass exchange between the tropics and subtropics on the interannual timescale. Instead of the general advection through the meridional overturning circulation, the advection of the spiciness anomalies at a certain isopycnal surface is another process that can demonstrate the effect of the subtropical variability on tropical climate (Zeller et al., 2021). Observations and model studies substantiate the existence of spiciness anomalies in the midlatitudes in both the North and South Pacific, which act as passive tracers to propagate toward the tropics along the geostrophic streamlines at isopycnal surfaces (Giese et al., 2002; Schneider, 2000; Yeager & Large, 2007; Zeller et al., 2021). But most works are of concern

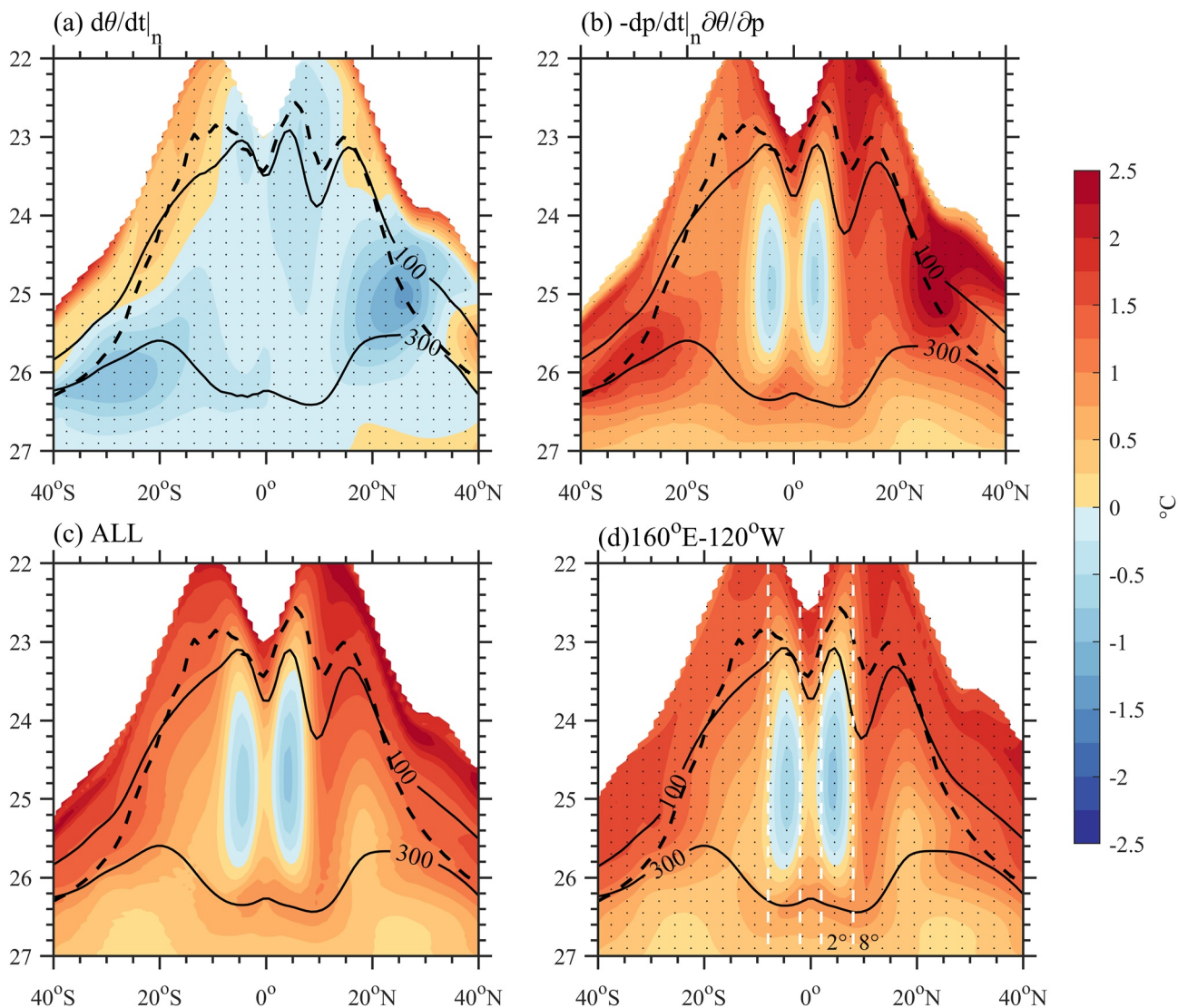


**Figure 4.** Contributions from (a) spiciness anomalies and (b) thermocline heave to isobaric temperature variability. The sum of two contributions is shown in (c), and (d) the temperature trend from 1950 to 2100 under the potential density coordinate. All value is the average over  $160^{\circ}\text{E}$ – $120^{\circ}\text{W}$ . Black dash contour represents the mixed layer depth in late winter (March in the Northern hemisphere and September in the Southern hemisphere), and solid lines are 100 and 300 m, respectively. White dash lines in (d) represent the latitude range of the off-equatorial subsurface (OES) region. The MLD is defined as the depth at which the water density is  $0.125 \text{ kg m}^{-3}$  larger than that at a depth of 5 m. Stippling indicates regions where the trends pass the 95% confidence level (Student's *t* test).

on the seasonal and interdecadal timescales. The present study makes an effort to introduce propagation under the future warming scenario.

The maximum spiciness trends also appear in the subtropics on a longer timescale and are located on a denser isopycnal surface in the South Pacific than in the North Pacific (Figure 4a). Hence, we choose different density ranges of the isopycnal surface to find the spatial patterns of the trend and verify such propagation. Since spiciness anomalies are defined on isopycnals in this study, temperature and salinity anomalies are closely related through the equation of state for seawater (Clément et al., 2020; Rudnick & Martin, 2002). Thus, only the isopycnal temperature anomalies are shown as the spiciness anomalies in the present study. The center of spiciness anomalies is located around  $25^{\circ}\text{N}$  (S) in the eastern subtropics, and the bowl shape subtropical gyre connects the subtropical and tropical Pacific at  $24.5 < \sigma < 25.5 \text{ kg m}^{-3}$  ( $25.0 < \sigma < 26.0 \text{ kg m}^{-3}$ ) isopycnal surface in the North (South) Pacific (Figure 5).

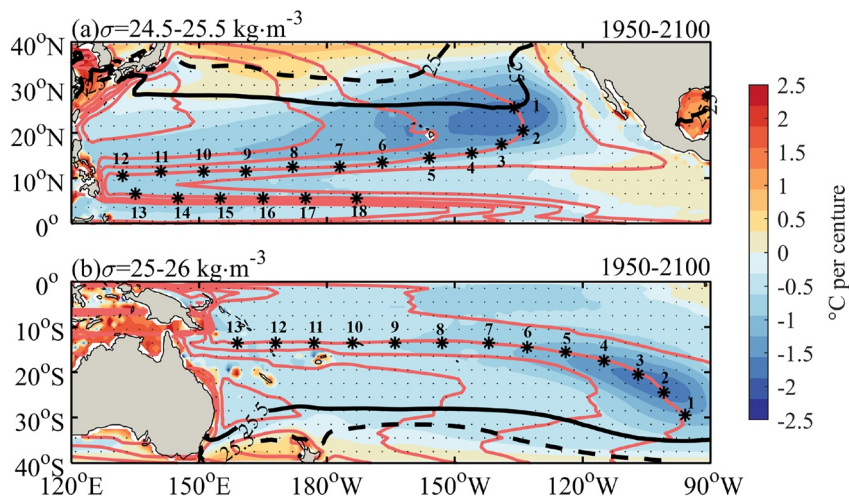


**Figure 5.** Long-term trend of temperature (shading,  $^{\circ}\text{C}$  per century) and mean streamline (red contours) on (a)  $24.5 < \sigma < 25.5$  and (b)  $25.0 < \sigma < 26.0$ . The asterisks are chosen to show the propagation of the cooling spiciness anomaly in a certain streamline. The black full (dash) line represents the location of the mixed layer based  $\sigma_{25.0}/\sigma_{25.5}$  in 1950–1970 (2080–2100) as the outcropping line. Stippling indicates regions where the trends pass the 95% confidence level (Student's *t* test).

Since the spiciness anomalies propagate clockwise (anticlockwise) along the subtropical gyre, we select some stations along a particular streamline of the subtropical gyre as the propagation pathway for these spiciness anomalies (Figure 5). The first station starts from the eastern subtropical cooling center, the last station ends in the tropical around  $5^{\circ}\text{N}$  ( $5^{\circ}\text{S}$ ), and the distance for the propagation pathway along the geostrophic streamline is approximately  $1.7 \times 10^4$  km ( $1.2 \times 10^4$  km) in the North (South) Pacific. It takes around 8.5(7) years for the cooling signals to propagate along the advection pathway in the North (South) Pacific (Figure 6), which suggests that the propagation has nearly the same rate ( $0.06/0.05 \text{ m}\cdot\text{s}^{-1}$ ) in both hemispheres. The cooling signals gradually weaken as they propagate due to diffusion (Figure 6). As a result, the tropical cooling trends partly originate from the continuously cooling signal in the eastern subtropical Pacific, especially in the future scenario. Previous studies suggested that variations in the ocean circulation strength, rather than variations in water properties carried by the circulation, are more likely to affect (Sasaki et al., 2010) variations in the equatorial SST, and the weakening anomalies might not continue along the equator due to the equatorial upwelling (Johnson et al., 2006; Luo et al., 2005; Nonaka et al., 2002). However, Li et al. (2012) claimed that despite the further slack anomalies, their arrival considerably contributes to the low-frequency spiciness variations in the central equatorial Pacific. We suppose that the subtropical spiciness anomalies might not efficiently impact the equatorial surface of the Pacific due to local strong vertical mixing process, but they could still play a significant role in the OES region.

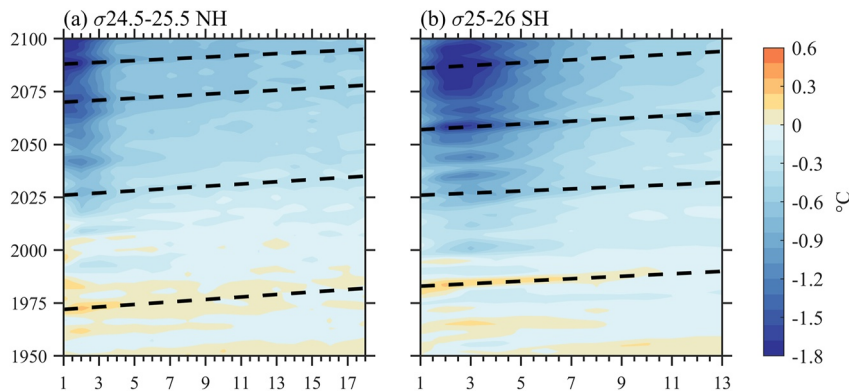


**Figure 6.** Time-station diagram of temperature change compared to 1950–1970 (shading,  $^{\circ}\text{C}$ ) averaged vertically over (a)  $24.5 < \sigma < 25.5$  and (b)  $25.0 < \sigma < 26.0$ . Horizontal axis represents the number of the asterisk in Figures 5a and 5b, respectively.

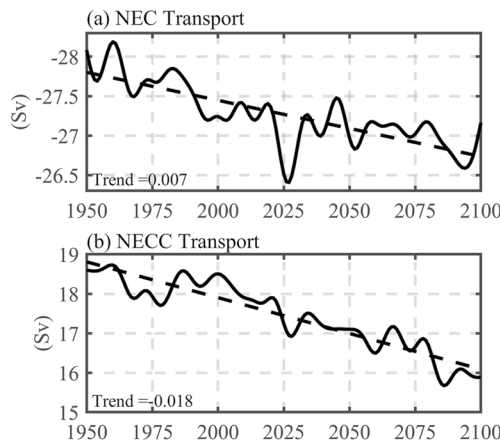


**Figure 7.** Time series of (a) North Equatorial Current's (NEC) transport in the zonal section of 9°–20°N and 125°E–120°W and (b) North Equatorial Countercurrent's (NECC) transport in the zonal section of 3°–8°N and 125°E–90°W. The unit of trend is Sv·yr<sup>-1</sup>. An 11-year low-pass filter has been applied to all the time series.

In the North Pacific, the water flows southward between 120° and 150°W and then westward along the North Equatorial Current (NEC) between 10° and 20°N to the western boundary, as the southern part of the subtropical circulation, and then eastward through the North Equatorial Countercurrent (NECC), as the component of tropical circulation (Figure 5). Under global warming, the zonal integrated NEC and NECC transports show decreasing trends from 1950 to 2100 (Figures 7a, 7b and Figure S4b in Supporting Information S1), suggesting that the water volume transmitted from the eastern subtropics to the tropics has decreased. Some works indicate that it is mainly a response to the weakening of the Walker circulation (Luo & Rothstein, 2011; Vecchi & Soden, 2007). It is well established that wind is the major force driving the upper ocean circulation in the tropical Pacific. Specifically, the decrease in wind stress curl intensity causes a weakening of the NEC and NECC (Figure 8a). The weakening of NEC and NECC is also associated with the reduced meridional sea surface height (SSH) gradient (not shown), governed by the convergence/divergence of anomalous Ekman transports (Figure 8b), which is consistent with the previous studies (Chen et al., 2016; Qiu & Chen, 2012). In the South Pacific, the water from the eastern subtropics flows to the tropics mainly through the South Equatorial Current (SEC) as the broad westward geostrophic flow in the northern limb of the subtropical circulation. The SEC around 10°S is also weakening (Figure 7a), resembling

the result in the North Pacific where the reduced water is transmitted to the tropics. Each model can hardly simulate the South Equatorial Countercurrent (SECC, Figure S3 in Supporting Information S1), and it may not reach the depth of the  $\sigma_{25.5}$  isopycnal surface, so we neglect the effect of SECC. In conclusion, although the ocean currents transport less water to the tropics, the negative spiciness trend still exists in the OES region, to some extent, suggesting that the propagation of subtropical maximum negative spiciness signal toward the equator by the mean current is indispensable.

#### 4.2. Thermocline Heave

Besides the spiciness process, the thermocline heave is another factor to modulate the temperature at a fixed depth. The isopycnal surfaces between  $\sigma_{24.0}$  and  $\sigma_{26.0}$  (about 100–300 m) all become shallower in 2°–7°N (S) and

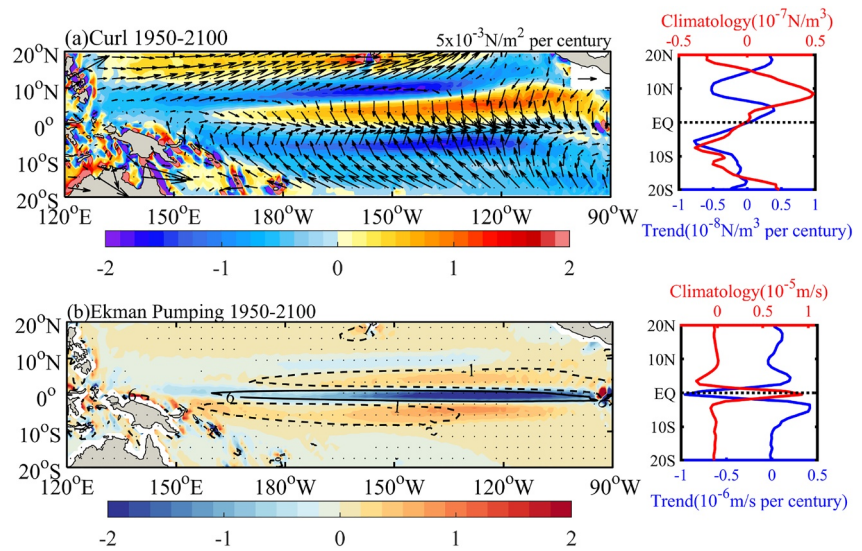


**Figure 8.** (left) Trends of (a) near-surface wind stress curl (shading,  $\times 10^{-8} \text{ N}\cdot\text{m}^{-3} \text{ per century}$ ) and wind stress (quiver,  $\text{N}\cdot\text{m}^{-2} \text{ per century}$ ) and (b) Ekman pumping (shading,  $\times 10^{-6} \text{ m s}^{-1} \text{ per century}$ ). Black lines in (b) show the climatology of Ekman pumping ( $\times 10^{-6} \text{ m s}^{-1}$ ). (right) Zonally averaged trend (blue) and climatology (red) of (a) near-surface wind stress curl and (b) Ekman pumping. Stippling indicates regions where the trends pass the 95% confidence level (Student's *t* test).

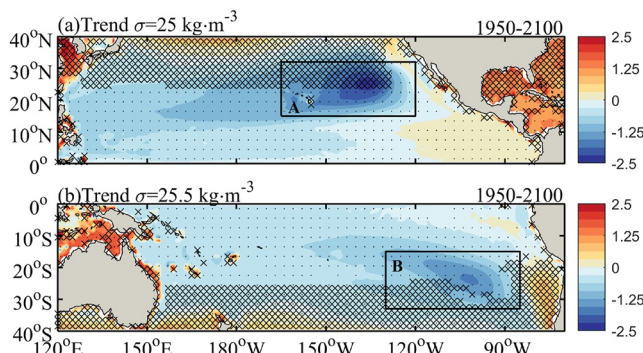


**Figure 9.** Temperature trends (shading,  $^{\circ}\text{C}$  per century) on (a)  $\sigma 25.0$  and (b)  $\sigma 25.5$  isopycnals. Hatching indicates the region affected by the late winter mixed layer. Stippling indicates regions where the trends pass the 95% confidence level (Student's *t* test). Region A is located in  $15^{\circ}$ – $32^{\circ}\text{N}$  and  $165^{\circ}$ – $120^{\circ}\text{W}$ . Region B is located in  $15^{\circ}$ – $33^{\circ}\text{S}$  and  $130^{\circ}$ – $85^{\circ}\text{W}$ .

It remains a question of how the long-term negative spiciness trend in the eastern subtropics generates. Although spiciness anomalies do not affect ocean dynamics, they can influence air-sea interaction when they arrive at the sea surface (Schneider, 2000). Therefore, it is necessary to explore their generation. We select two certain isopycnal surfaces that the eastern subtropical spiciness trends reach their maximum, that is,  $\sigma 25.0$  isopycnal surface in the North Pacific and  $\sigma 25.5$  isopycnal surface in the South Pacific. The late winter outcropping regions cover part of the maximum negative spiciness trend region in both the northeastern and southeastern subtropics. This implies that, on the one hand, the mixing process within the mixed layer may affect the generation of spiciness anomalies. On the other hand, beneath the mixed layer, the subsurface process may also play an important role in the Pacific (Yeager & Large, 2004). The largest trend is generated between  $15^{\circ}$  and  $30^{\circ}\text{N}$  in the North Pacific and in the same latitude range but with denser isopycnal in the South Pacific (Figure 9). Signals appear stronger in the North Pacific, with an average of  $-1.16$  ( $-0.80$ )  $^{\circ}\text{C}$  per century and a maximum of  $-2.12$  ( $-1.55$ )  $^{\circ}\text{C}$  per century in Region A (B; shown in Figure 9). Diapycnal mixing is more active on denser isopycnal surface in the South Pacific, which is sufficiently vigorous to reduce the anomalies after generation (Johnson, 2006), concurring with the weaker anomalies. The strength of the spiciness trends weakens to the west and equator, which elucidates the subsequent propagation and diffusion to some extent (Figure 9).

Above all, spiciness anomalies can primarily be generated by three mechanisms. (a) The anomalous signals are directly subducted from outcropping lines. Given the meridional density compensating distribution in the Pacific, SST anomalies cause the migration of the outcropping lines and the associated changes in the temperature and salinity properties, thus inducing the thermohaline anomaly on isopycnal surfaces (Nonaka & Sasaki, 2007). (b) Anomalous advection across a mean isopycnal T-S front. Anomalous ocean currents forced by anomalous wind stress curl displace the temperature front on isopycnals, which causes temperature anomalies on isopycnals, hence spiciness anomalies (Schneider, 2000). (c) The diapycnal mixing at the base of the surface mixed layer (spice injection mechanism). Spice injection can only occur with weak stratification and destabilizing salinity. Such conditions lead to a strong diapycnal flux of salt and temperature at the base of a penetrating convective boundary layer, which locates between the mixed layer and thermocline with strong compensated density, and finally produces significant variability on isopycnal surfaces (Kolodziejczyk & Gaillard, 2013; Wang et al., 2020; Yeager & Large, 2004, 2007). As a result, spice injection can only generate positive spiciness anomalies over the eastern subtropics. It is thus not able to contribute to the generation of the negative spiciness anomalies in the present study. Wang (2020) also indicated a significant negative correlation between variations in spiciness generation and local SST. The SST increases, and upper ocean stratification enhances in the tropical/subtropical Pacific under global warming (Capotondi et al., 2012; Xie et al., 2010). As a result, the negative spice injection process may hardly occur under a warming climate. Thus, the present study mainly focuses on the first two mechanisms.

The ventilation thermocline theory indicates that the transmission of the surface properties into the interior thermocline is mainly through the lateral penetration along the isopycnal surfaces (Luyten et al., 1983; Robbins

cover almost the entire Pacific basin, while the negative depth trend of  $\sigma 26.0$  isopycnal surface shrinks to a tiny area in the eastern off-equatorial region (Figures S5 and S6 in Supporting Information S1). This may be induced by significant wind stress curl changes off the equator, where a positive trend is seen to the north and a negative trend to the south (Figure 8a). The wind stress curl determines the local Ekman pumping, causing the vertical motion to affect the thermocline depth. We use the formulas in Wang et al. (2019) to obtain the near-equatorial Ekman transports. The positive (negative) wind stress curl trends in the northern (southern) off-equatorial region ( $2^{\circ}$ – $7^{\circ}\text{N/S}$ ) cause divergence, which in turn lead to anomalous upwelling and a shoaling of the thermocline depth (Figure 8b). The upwelling takes the colder water upward, contributing to the cooling trend at a fixed depth in the OES region.

#### 4.3. Spiciness Generation

In the past section, we elucidate two impact factors of the negative temperature trend in the subsurface tropical Pacific and illustrate the origin of the tropical spiciness trend as well as the drivers of the local thermocline heave.

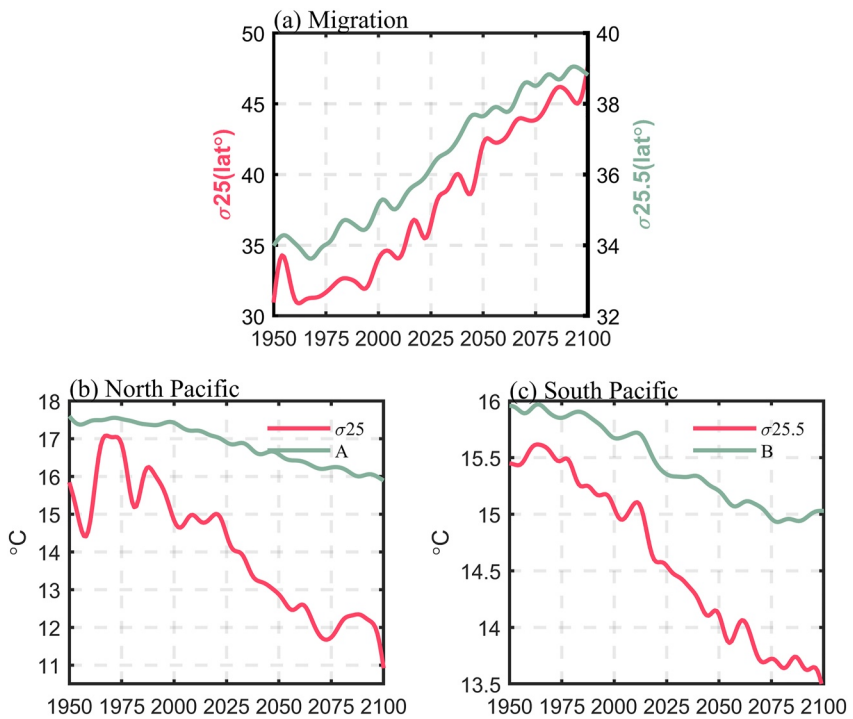


**Figure 10.** Time series of (a) latitude of  $\sigma_{25.0}$  over  $155^{\circ}$ – $125^{\circ}\text{W}$  (red line) in the North Pacific and  $\sigma_{25.5}$  over  $120^{\circ}$ – $90^{\circ}\text{W}$  (green line) in the South Pacific; and (b) average temperature of  $\sigma_{25.0}$  in the area mentioned in (a) and Region A in Figure 9, (c)  $\sigma_{25.5}$  in the area mentioned in (a) and Region B in Figure 9. The two isopycnals in the late winter mixed layer base are used as the outcropping lines. An 11-year low-pass filter has been applied to all the time series.

et al., 2000). Figure 5 shows that the subtropical streamlines pass through the outcropping region, suggesting that the properties in the mixed layer can be directly advected to the eastern subsurface ocean by ventilating flow. Meanwhile, numerous studies demonstrate that the outcropping lines in the Pacific migrate poleward consistently under global warming in the climate models (Wang et al., 2015). The temperature and salinity both have negative gradients toward higher latitude in the Pacific, so the poleward migration of the outcropping lines means that the water advected through the isopycnal surfaces becomes cooler. Under the SSP2-4.5 scenario, the  $\sigma_{25.0}$  outcropping line moves from approximately  $28^{\circ}\text{N}$  to  $40^{\circ}\text{N}$  in the eastern North Pacific, and  $\sigma_{25.5}$  outcropping line moves from approximately  $31^{\circ}\text{S}$  to  $48^{\circ}\text{S}$  in the eastern South Pacific from 1950 to 2100 (Figure 10a). According to Xie (2010), there is a tendency for greater warming in the northern Pacific subtropics than in the southern Pacific subtropics in accordance with asymmetries in the trade wind changes. It may be why the outcropping line in the North Pacific migrates more degrees than that in the South Pacific. To discuss the effect of the poleward migration of outcropping lines, equivalently, the subduction process, the temperature at the base of the mixed layer along the outcropping lines is used to compare with the temperature at the same potential density surface in Region A and B, respectively. The temperature continuously decreases in the outcropping lines because of the lower temperature in higher latitudes (Figures 10b and 10c). Temperature change reaches  $4.7\ ^{\circ}\text{C}$  ( $1.7\ ^{\circ}\text{C}$ ) at  $\sigma_{25.0}$  ( $\sigma_{25.5}$ ) outcropping line in the northeastern (southeastern) Pacific, while only reaches  $2\ ^{\circ}\text{C}$  ( $1\ ^{\circ}\text{C}$ ) in Region A (B; Figures 10b and 10c). Furthermore, the negative trends in Regions A and B are both much smaller than that at outcropping lines (Figures 10b and 10c). We consider that the depth of the  $\sigma_{25.0}$  ( $\sigma_{25.5}$ ) isopycnal surface is lower than the depth of the local mixed layer in the northern (southern) part of Region A (B), where the intense mixing process may largely recede the cooling signal carried by the subducted water (Cerovečki et al., 2013, 2016).

However, the poleward migration of the outcropping line is not the only driver of the negative spiciness trend due to the dissipation within the mixed layer. The present study further considers the effect of the advection process. The temperature change at a particular isopycnal surface can be induced by advection through heat convergence/divergence. As Schneider (2000) shows the spatial patterns of the current trend and climatology temperature to provide the details of the advection process. There is a warm core around  $25^{\circ}\text{N}$  in the central North Pacific, and

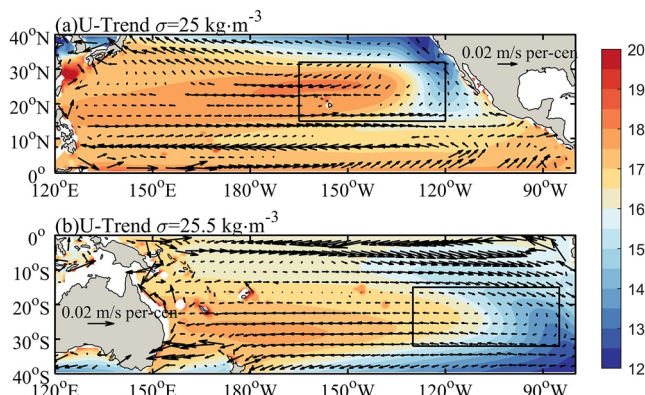


**Figure 11.** The mean temperature (shading,  $^{\circ}\text{C}$ ) and the current trend (vectors,  $\text{m s}^{-1}$  per century) at (a)  $\sigma25.0$  and (b)  $\sigma25.5$  isopycnals. The mean and trend are both calculated from 1950 to 2100. The shown vectors indicate the trends pass the 95% confidence level (Student's  $t$  test).

temperature in Region A is part of the warm core with an average of  $17.4\ ^{\circ}\text{C}$  (Figure 11a). A prominent south-westward current trend occurs between  $25^{\circ}\text{N}$  and  $30^{\circ}\text{N}$  and  $140^{\circ}\text{--}170^{\circ}\text{W}$ , which displaces a temperature front around the northern boundary of Region A. It brings the cold water from the high latitude to the eastern subtropics at  $\sigma25.0$  isopycnal surface and then causes the subsurface cooling spiciness here. However, the warm core lies around  $30^{\circ}\text{S}$  in the western South Pacific, and the climatology temperature in Region B is  $15\ ^{\circ}\text{C}$  (Figure 11b). The subtropical circulation has a clockwise trend in the South Pacific, suggesting a general weakening at  $\sigma25.5$  isopycnal surface. The meridional (southward) current trend mostly exists around the northern boundary of Region B, where the mean temperature gradient is positive. The zonal (westward) current trend largely occurs around the southern boundary, taking eastern cooler water to this region (Figure 11b). These two processes may partly offset each other, so the anomalous current may not be the major factor in inducing the negative spiciness trend in the South Pacific Wood (1985).

To further investigate the overall effect of the oceanic advection, we decompose the contribution into three impact factors as ocean current change, temperature gradient change, and nonlinear term (Equations 3 and 4) and

quantitatively analyze them separately. We investigate the zonal and meridional advection of two distinct isopycnal surfaces in the Pacific. For Region A in the northeastern Pacific, while zonal advection change exerts a warming effect, the meridional advection change contributes to stronger cooling (Figure 12). As a result, the total horizontal advection induces a cooling effect in Region A, reaching  $-2.41\ ^{\circ}\text{C}$  per century. To elaborate, the anomalous cooling from the meridional advection is dominated by the cooling effect of the anomalous southward current in the northern boundary of Region A, just as Figure 11a shows. The anomalous southward current transmits cooler water to the region, and the subsequent circulation carries cooler mixed layer water into the subsurface. For Region B in the southeastern Pacific, the cooling effect of meridional advection exceeds the warming effect of zonal advection, and the total cooling effect can reach  $-1.12\ ^{\circ}\text{C}$  per century. It is worth noting that the change in horizontal temperature gradient contributes a lot to both the zonal and meridional advection. The ocean current change plays a secondary role, consistent with the result from Figure 11. The zonal and meridional nonlinear terms seem to offset each other in both the northeastern and southeastern Pacific. More importantly, the negative contribution of the meridional temperature gradient change (Figure 12, blue bars in second and fourth panels) can reflect the effect of poleward migration of outcropping lines to some extent. The contribution of the temperature gradient change indeed seems quantitatively small in the North Pacific, compared to the contribution of the ocean current change, but it is of the same order of magnitude as the temperature change in Region A. In addition, roughly half of Region A is contained in the outcropping region (Figure 9). Its influence on the characteristics of water mass transferred from the surface mixed layer could be indispensable. In the South Pacific, the poleward migration of outcropping lines is a significant factor in the negative spiciness trend (Figure 12).

In summary, poleward migration of outcropping lines contributes to the subtropical negative spiciness trends in both hemispheres but is more important in the South Pacific. The meridional advection anomalies through the anomalous southward currents contribute to the negative spiciness trends in Region A, and the meridional temperature gradient changes contribute to the negative spiciness trends in Region B, respectively.

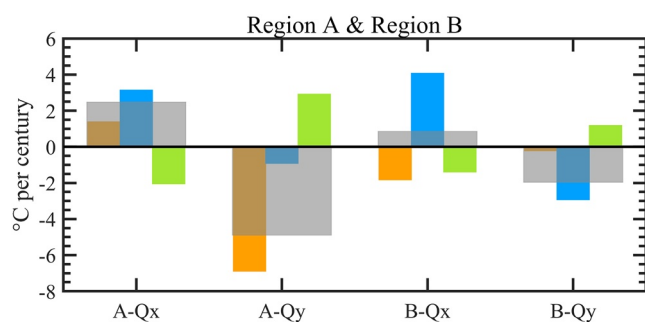


**Figure 12.** Oceanic advection changes ( $^{\circ}\text{C}$  per century) in (left two panels) Region A at  $\sigma25.0$  isopycnal surface and (right two panels) Region B at  $\sigma25.5$  isopycnal surface.  $Q_x$  and  $Q_y$  are the zonal and meridional advection, with each of them (gray bar) being decomposed into ocean current change (orange bar), temperature gradient change (blue bar), and nonlinear term (green bar). A mean from 1950 to 2100 is taken for analysis.

## 5. Discussion and Conclusion

Based on the investigation from 14 models in CMIP6, two robust symmetric subsurface cooling trends are shown in the tropical Pacific off-equatorial region ( $2^{\circ}\text{--}8^{\circ}\text{N/S}$ ) under the SSP2-4.5 scenario. The temperature trend at the fixed level can be decomposed into contributions from spiciness variation and thermocline heave. Previous studies only discussed the contribution of

the thermocline heave, namely, the deepening/shoaling of the thermocline, or the direct radiative effect (Luo et al., 2011, 2018), while the present study finds that spiciness variation is as significant as thermocline heave in the tropical subsurface region, so we emphasize the contribution of the spiciness variation. The maximum negative spiciness trends appear in the eastern subtropics in both the North and South Pacific. These subtropical maximum trends will propagate westward and equatorward along streamlines at the certain isopycnal surface to the tropics on the decadal time scale. The subsurface spiciness trend can alter the vertical temperature structure in the tropics, although it does not have a significant impact on SST. Despite weakening NEC/NECC in the North Pacific and the SEC in the South Pacific, the cooling signals are still transmitted to the tropics, suggesting the dominant factor of the cooling water transported by the mean circulation instead of the circulation anomalies. When it comes to the effect of the thermocline heave, the great wind stress curl change in the off-equatorial region with upward Ekman pumping leads to a shoaling of the tropical thermocline.

In the Pacific, the original spiciness trends are generated in the eastern subtropics, in conjunction with past studies on the seasonal, interannual to decadal time scales (Kolodziejczyk & Gaillard, 2012, 2013; Luo et al., 2005; Wang & Luo, 2020; Yeager & Large, 2004). First, our results show that the outcropping lines migrate poleward consistently in both hemispheres under global warming. The flows along the isopycnal surface directly transmit the cooler surface water from higher latitudes to the subtropical interior thermocline, causing the negative spiciness trends in the North and South Pacific (Laurian et al., 2009; Nonaka & Sasaki, 2007). Furthermore, the oceanic advection can also exert subsurface temperature anomalies. Anomalous meridional advects in the northeastern and southeastern Pacific contribute significantly to the subtropical negative spiciness trends. In the North Pacific, anomalous ocean currents displace the temperature front on the isopycnals to induce a cooling trend, while in the South Pacific, the anomalous temperature gradients lead to the cooling trend. Besides, the subtropical region with the maximum spiciness in the North and South Pacific is partly across the outcropping region. Thus, the strong vertical mixing process in the mixed layer may largely impair the effect of the subduction and advection.

In addition, numerous previous studies have demonstrated that the injection process may be the main reason to cause the positive spiciness anomalies in the South Pacific (Kolodziejczyk & Gaillard, 2012; Wang & Luo, 2020; Yeager & Large, 2004, 2007). Nevertheless, despite the great significance of the spice injection, it is proved not able to contribute to the generation of negative spiciness anomalies (Kolodziejczyk & Gaillard, 2013; Wang & Luo, 2020).

## Data Availability Statement

All outputs from the CMIP6 are available on <https://esgf-node.ipsl.upmc.fr/search/cmip6-ipsl/>. The ARGO data sets are available on [http://sio-argo.ucsd.edu/RG\\_Climatology.html](http://sio-argo.ucsd.edu/RG_Climatology.html). The EN4 data sets are available on <https://www.metoffice.gov.uk/hadobs/en4/download-en4-2-1.html>. The IAP products are downloaded from <http://www.ocean.iap.ac.cn/pages/dataService/dataService.html?navAnchor=dataService>. The Ishii data are taken from <https://rda.ucar.edu/datasets/ds285.3/index.html#sf01-wl-/data/ds285.3?g=11>.

## Acknowledgments

This work is supported by the National Natural Science Foundation of China (42090042), the Southern Marine Science and Engineering Guangdong Laboratory (Guangzhou; GML2019ZD0303, 2019BT02H594), and the Chinese Academy of Sciences (133244KYSB20190031, ISEE2021PY02, and ISEE2021ZD01).

## References

- Andrews, T., & Webb, M. J. (2018). The dependence of global cloud and lapse rate feedbacks on the spatial structure of tropical Pacific warming. *Journal of Climate*, 31(2), 641–654. <https://doi.org/10.1175/JCLI-D-17-0087.1>
- Arbic, B. K., & Owens, W. B. (2001). Climatic warming of Atlantic intermediate waters. *Journal of Climate*, 14(20), 4091–4108. [https://doi.org/10.1175/1520-0442\(2001\)014<4091:CWOAIW>2.0.CO;2](https://doi.org/10.1175/1520-0442(2001)014<4091:CWOAIW>2.0.CO;2)
- Bindoff, N. L. (2019). Change ocean, marine ecosystems, and dependent communities. In H.-O. Pörtner, D. C., Roberts, V., Mason Delmotte, P., Zhai, M., Tignor, & E., Poloczanska (Eds.), *IPCC special report on the ocean and cryosphere in a changing climate* (pp. 447–588).
- Bindoff, N. L., & McDougall, T. J. (1994). Diagnosing climate change and ocean ventilation using hydrographic data. *Journal of Physical Oceanography*, 24(6), 1137–1152. [https://doi.org/10.1175/1520-0485\(1994\)024<1137:DCCAOV>2.0.CO;2](https://doi.org/10.1175/1520-0485(1994)024<1137:DCCAOV>2.0.CO;2)
- Boyer, T. P., Antonov, J. I., Baranova, O. K., Coleman, C., Garcia, H. E., Grodsky, A., et al. (2013). World Ocean Database 2013 (NOAA Atlas NESDIS 72, p. 209). NOAA Atlas.
- Bratcher, A. J., & Giese, B. S. (2002). Tropical Pacific decadal variability and global warming. *Geophysical Research Letters*, 29(19), 1918. <https://doi.org/10.1029/2002GL015191>
- Capotondi, A., Alexander, M. A., Bond, N. A., Curchitser, E. N., & Scott, J. D. (2012). Enhanced upper ocean stratification with climate change in the CMIP3 models. *Journal of Geophysical Research*, 117, C04031. <https://doi.org/10.1029/2011JC007409>
- Cerovečki, I., & Mazloff, M. R. (2016). The spatiotemporal structure of diabatic processes governing the evolution of Subantarctic Mode Water in the Southern Ocean. *Journal of Physical Oceanography*, 46(2), 683–710. <https://doi.org/10.1175/JPO-D-14-0243.1>

- Cerovečki, I., Talley, L. D., Mazloff, M. R., & Maze, G. (2013). Subantarctic mode water formation, destruction, and export in the eddy-permitting Southern Ocean state estimate. *Journal of Physical Oceanography*, 43(7), 1485–1511. <https://doi.org/10.1175/JPO-D-12-0121.1>
- Chen, X., Qiu, B., Du, Y., Chen, S., & Qi, Y. (2016). Interannual and interdecadal variability of the north equatorial Countercurrent in the Western Pacific. *Journal of Geophysical Research: Oceans*, 121, 7743–7758. <https://doi.org/10.1002/2016JC012190>
- Cheng, L., & Zhu, J. (2016). Benefits of CMIP5 multi-model ensemble in reconstructing historical ocean subsurface temperature variations. *Journal of Climate*, 29(15), 5393–5416. <https://doi.org/10.1175/JCLI-D-15-0730.1>
- Church, J. A., Godfrey, J. S., Jackett, D. R., & McDougall, T. J. (1991). A model of sea level rise caused by ocean thermal expansion. *Journal of Climate*, 4(4), 438–456. [https://doi.org/10.1175/1520-0442\(1991\)004<438:AMOSLR>2.0.CO;2](https://doi.org/10.1175/1520-0442(1991)004<438:AMOSLR>2.0.CO;2)
- Clément, L., McDonagh, E. L., Marzocchi, A., & Nurser, A. J. G. (2020). Signature of ocean warming at the mixed layer base. *Geophysical Research Letters*, 47, e2019GL086269. <https://doi.org/10.1029/2019GL086269>
- Du, Y., & Xie, S. P. (2008). Role of atmospheric adjustments in the tropical Indian Ocean warming during the 20th century in climate models. *Geophysical Research Letters*, 35, L08712. <https://doi.org/10.1029/2008GL033631>
- Eyring, V., Bony, S., Meehl, G. A., Senior, C. A., Stevens, B., Stouffer, R. J., & Taylor, K. E. (2016). Overview of the coupled model intercomparison Project Phase 6 (CMIP6) experimental design and organization. *Geoscientific Model Development*, 9(5), 1937–1958. <https://doi.org/10.5194/gmd-9-1937-2016>
- Flato, G., Marotzke, J., Abiodun, B., Braconnot, P., Chou, S. C., Collins, W., et al. (2013). Evaluation of climate models. In T. F. Stocker, D. Qin, G.-K., Plattner, M., Tignor, S. K., Allen, & J., Boschung (Eds.), *Climate change 2013: The physical science basis. Contribution of working group I to the fifth assessment report of the intergovernmental panel on climate change* (pp. 741–866). Cambridge University Press.
- Giese, B. S., Urizar, S. C., & Fučkar, N. S. (2002). Southern hemisphere origins of the 1976 climate shift. *Geophysical Research Letters*, 29(2), 1014. <https://doi.org/10.1029/2001GL013268>
- Good, S. A., Martin, M. J., & Rayner, N. A. (2013). EN4: Quality controlled ocean temperature and salinity profiles and monthly objective analyses with uncertainty estimates. *Journal of Geophysical Research: Oceans*, 118, 6704–6716. <https://doi.org/10.1002/2013JC009067>
- Gu, D., & Philander, S. G. H. (1997). Interdecadal climate fluctuations that depend on exchanges between the tropics and extratropics. *Science*, 275(5301), 805–807. <https://doi.org/10.1126/science.275.5301.805>
- Häkkinen, S., Rhines, P. B., & Worthen, D. L. (2016). Warming of the global ocean: Spatial structure and water-mass trends. *Journal of Climate*, 29(13), 4949–4963. <https://doi.org/10.1175/JCLI-D-15-0607.1>
- Ishii, M., Kimoto, M., Sakamoto, K., & Iwasaki, S. (2005). *Subsurface temperature and salinity analyses*. Research Data Archive at the National Center for Atmospheric Research, Computational and Information Systems Laboratory. <https://doi.org/10.5065/Y6CR-KW66>
- Johnson, G. C. (2006). Generation and initial evolution of a mode water θ-S anomaly. *Journal of Physical Oceanography*, 36(4), 739–751. <https://doi.org/10.1175/JPO2895.1>
- Johnson, G. C., & Lyman, J. M. (2020). Warming trends increasingly dominate global ocean. *Nature Climate Change*, 10(8), 757–761. <https://doi.org/10.1038/s41558-020-0822-0>
- Kakatkar, R., Gnanaseelan, C., & Chowdary, J. S. (2020). Asymmetry in the tropical Indian Ocean subsurface temperature variability. *Dynamics of Atmospheres and Oceans*, 90(4), 101142. <https://doi.org/10.1016/j.dynatmoce.2020.101142>
- Kleeman, R., McCreary, J. P., & Klinger, B. A. (1999). A mechanism for generating ENSO decadal variability. *Geophysical Research Letters*, 26(12), 1743–1746. <https://doi.org/10.1029/1999GL900352>
- Kolodziejczyk, N., & Gaillard, F. (2012). Observation of spiciness interannual variability in the Pacific pycnocline. *Journal of Geophysical Research*, 117, C12018. <https://doi.org/10.1029/2012JC008365>
- Kolodziejczyk, N., & Gaillard, F. (2013). Variability of the heat and salt budget in the subtropical southeastern Pacific mixed layer between 2004 and 2010: Spice injection mechanism. *Journal of Physical Oceanography*, 43(9), 1880–1898. <https://doi.org/10.1175/JPO-D-13-041>
- Laurian, A., Lazar, A., & Reverdin, G. (2009). Generation mechanism of spiciness anomalies: An OGCM analysis in the North Atlantic subtropical gyre. *Journal of Physical Oceanography*, 39(4), 1003–1018. <https://doi.org/10.1175/2008JPO3896.1>
- Levitus, S., Antonov, J., & Boyer, T. (2005). Warming of the world ocean, 1955–2003. *Geophysical Research Letters*, 32, L02604. <https://doi.org/10.1029/2004GL021592>
- Levitus, S., Antonov, J. I., Boyer, T. P., Baranova, O. K., Garcia, H. E., Locarnini, R. A., et al. (2012). World ocean heat content and thermosteric sea level change (0–2000 m), 1955–2010. *Geophysical Research Letters*, 39, L10603. <https://doi.org/10.1029/2012GL051106>
- Li, Y., & Wang, F. (2015). Thermocline spiciness variations in the tropical Indian Ocean observed during 2003–2014. *Deep-Sea Research Part I: Oceanographic Research Papers*, 97, 52–66. <https://doi.org/10.1016/j.dsr.2014.12.004>
- Li, Y., Wang, F., & Sun, Y. (2012). Low-frequency spiciness variations in the tropical Pacific Ocean observed during 2003–2012. *Geophysical Research Letters*, 39, L23601. <https://doi.org/10.1029/2012GL053971>
- Luo, Y., Liu, F., & Lu, J. (2018). Response of the equatorial Pacific thermocline to climate warming. *Ocean Dynamics*, 68(11), 1419–1429. <https://doi.org/10.1007/s10236-018-1209-x>
- Luo, Y., & Rothstein, L. M. (2011). Response of the Pacific Ocean circulation to climate change. *Atmosphere-Ocean*, 49(3), 235–244. <https://doi.org/10.1080/07055900.2011.602325>
- Luo, Y., Rothstein, L. M., Zhang, R. H., & Busalacchi, A. J. (2005). On the connection between South Pacific subtropical spiciness anomalies and decadal equatorial variability in an ocean general circulation model. *Journal of Geophysical Research*, 110, C10002. <https://doi.org/10.1029/2004JC002655>
- Luyten, J., Pedlosky, J., & Stommel, H. (1983). Climatic inferences from the ventilated thermocline. *Climatic Change*, 5, 183–191. <https://doi.org/10.1007/BF02423489>
- Lyu, K., Zhang, X., & Church, J. A. (2020). Regional dynamic sea level simulated in the CMIP5 and CMIP6 models: Mean biases, future projections, and their linkages. *Journal of Climate*, 33(15), 6377–6398. <https://doi.org/10.1175/JCLI-D-19-1029.1>
- Ma, J., & Xie, S. P. (2013). Regional patterns of sea surface temperature change: A Source of uncertainty in future projections of precipitation and atmospheric circulation. *Journal of Climate*, 26(8), 2482–2501. <https://doi.org/10.1175/JCLI-D-12-00283.1>
- McCreary, J. P., & Peng, L. (1994). Interaction between the subtropical and equatorial ocean circulations: The subtropical cell. *Journal of Physical Oceanography*, 24(2), 466–497. [https://doi.org/10.1175/1520-0485\(1994\)024<466:IBTSAE>2.0.CO;2](https://doi.org/10.1175/1520-0485(1994)024<466:IBTSAE>2.0.CO;2)
- McKenna, S., Santoso, A., Gupta, A. S., & Cai, W. (2020). Indian ocean dipole in CMIP5 and CMIP6: Characteristics, biases, and links to ENSO. *Scientific Reports*, 10(1), 1–13. <https://doi.org/10.1038/s41598-020-68268-9>
- Munk, W. (1981). Internal waves and small scale processes. In B. A. Warrant, & C. Wunsch (Eds.), *Evolution of physical oceanography* (pp. 264–291). MIT Press.
- Nagura, M., & Kouketsu, S. (2018). Spiciness anomalies in the upper south Indian ocean. *Journal of Physical Oceanography*, 48(9), 2081–2101. <https://doi.org/10.1175/JPO-D-18-0050.1>

- Nonaka, M., & Sasaki, H. (2007). Formation mechanism for isopycnal temperature-salinity anomalies propagating from the Eastern South Pacific to the Equatorial region. *Journal of Climate*, 20(7), 1305–1315. <https://doi.org/10.1175/JCLI4065.1>
- Nonaka, M., Xie, S. P., & McCreary, J. P. (2002). Decadal variations in the subtropical cells and equatorial Pacific SST. *Geophysical Research Letters*, 29(7), 201–204. <https://doi.org/10.1029/2001GL013717>
- Palmer, M. D., Harris, G. R., & Gregory, J. M. (2018). Extending CMIP5 projections of global mean temperature change and sea level rise due to thermal expansion using a physically-based emulator. *Environmental Research Letters*, 13(8), 84003. <https://doi.org/10.1088/1748-9326/aad2e4>
- Qiu, B., & Chen, S. (2012). Multidecadal sea level and Gyre circulation variability in the Northwestern tropical Pacific ocean. *Journal of Physical Oceanography*, 42(1), 193–206. <https://doi.org/10.1175/JPO-D-11-061.1>
- Robbins, P. E., Price, J. F., Owens, W. B., & Jenkins, W. J. (2000). The importance of lateral diffusion for the ventilation of the lower thermocline in the subtropical North Atlantic. *Journal of Physical Oceanography*, 30(1), 67–89. [https://doi.org/10.1175/1520-0485\(2000\)030<0067:tioldf>2.0.co;2](https://doi.org/10.1175/1520-0485(2000)030<0067:tioldf>2.0.co;2)
- Roemmich, D., & Gilson, J. (2009). The 2004–2008 mean and annual cycle of temperature, salinity, and steric height in the global ocean from the Argo Program. *Progress in Oceanography*, 82(2), 81–100. <https://doi.org/10.1016/j.pocean.2009.03.004>
- Rudnick, D. L., & Martin, J. P. (2002). On the horizontal density ratio in the upper ocean. *Dynamics of Atmospheres and Oceans*, 36(1–3), 3–21. [https://doi.org/10.1016/S0377-0265\(02\)00022-2](https://doi.org/10.1016/S0377-0265(02)00022-2)
- Sasaki, Y. N., Schneider, N., Maximenko, N., & Lebedev, K. (2010). Observational evidence for propagation of decadal spiciness anomalies in the North Pacific. *Geophysical Research Letters*, 37, L07708. <https://doi.org/10.1029/2010GL042716>
- Schneider, E. K., Huang, B., Zhu, Z., Dewitt, D. G., Kinter, J. L., Kirtman, B. P., & Shukla, J. (1999a). Ocean data assimilation, initialization, and predictions of ENSO with a coupled GCM. *Monthly Weather Review*, 127(6 II), 1187–1207. [https://doi.org/10.1175/1520-0493\(1999\)127<1187:ODAIAP>2.0.CO;2](https://doi.org/10.1175/1520-0493(1999)127<1187:ODAIAP>2.0.CO;2)
- Schneider, N. (2000). A decadal spiciness mode in the tropics. *Geophysical Research Letters*, 27(2), 257–260. <https://doi.org/10.1029/1999GL002348>
- Schneider, N., Miller, A. J., Alexander, M. A., & Deser, C. (1999b). Subduction of decadal North Pacific temperature anomalies: Observations and dynamics. *Journal of Physical Oceanography*, 29(5), 1056–1070. [https://doi.org/10.1175/1520-0485\(1999\)029<1056:SODNPT>2.0.CO;2](https://doi.org/10.1175/1520-0485(1999)029<1056:SODNPT>2.0.CO;2)
- Shin, S. I., & Sardeshmukh, P. D. (2011). Critical influence of the pattern of Tropical Ocean warming on remote climate trends. *Climate Dynamics*, 36(7), 1577–1591. <https://doi.org/10.1007/s00382-009-0732-3>
- Sparks, N., & Toumi, R. (2020). Pacific subsurface ocean temperature as a long-range predictor of South China tropical cyclone landfall. *Communications Earth & Environment*, 1(1), 1–7. <https://doi.org/10.1038/s43247-020-00033-2>
- Tokinaga, H., Xie, S. P., Deser, C., Kosaka, Y., & Okumura, Y. M. (2012). Slowdown of the Walker circulation driven by tropical Indo-Pacific warming. *Nature*, 491(7424), 439–443. <https://doi.org/10.1038/nature11576>
- Vecchi, G. A., & Soden, B. J. (2007). Global warming and the weakening of the tropical circulation. *Journal of Climate*, 20(17), 4316–4340. <https://doi.org/10.1175/JCLI4258.1>
- Wang, G., Cheng, L., Abraham, J., & Li, C. (2018). Consensuses and discrepancies of basin-scale ocean heat content changes in different ocean analyses. *Climate Dynamics*, 50(7–8), 2471–2487. <https://doi.org/10.1007/s00382-017-3751-5>
- Wang, G., Xie, S. P., Huang, R. X., & Chen, C. (2015). Robust warming pattern of global subtropical oceans and its mechanism. *Journal of Climate*, 28(21), 8574–8584. <https://doi.org/10.1175/JCLI-D-14-00809.1>
- Wang, M., Du, Y., Qiu, B., Xie, S. P., & Feng, M. (2019). Dynamics on seasonal variability of EKE associated with TIWs in the eastern equatorial Pacific ocean. *Journal of Physical Oceanography*, 49(6), 1503–1519. <https://doi.org/10.1175/JPO-D-18-0163.1>
- Wang, Y., & Luo, Y. (2020). Variability of spice injection in the upper ocean of the southeastern Pacific during 1992–2016. *Climate Dynamics*, 54(5–6), 3185–3200. <https://doi.org/10.1007/s00382-020-05164-y>
- Woods, J. D. (1985). The physics of thermocline ventilation. *Elsevier Oceanography Series*, 40(C), 543–590. [https://doi.org/10.1016/S0422-9894\(08\)70730-X](https://doi.org/10.1016/S0422-9894(08)70730-X)
- Xie, S. P., Deser, C., Vecchi, G. A., Ma, J., Teng, H., & Wittenberg, A. T. (2010). Global warming pattern formation: Sea surface temperature and rainfall. *Journal of Climate*, 23(4), 966–986. <https://doi.org/10.1175/2009JCLI3329.1>
- Yang, H., Wang, F., & Sun, A. (2009). Understanding the ocean temperature change in global warming: The tropical Pacific. *Tellus, Series A: Dynamic Meteorology and Oceanography*, 61(3), 371–380. <https://doi.org/10.1111/j.1600-0870.2009.00390.x>
- Yeager, S. G., & Large, W. G. (2004). Late-winter generation of spiciness on subducted isopycnals. *Journal of Physical Oceanography*, 34(7), 1528–1547. [https://doi.org/10.1175/1520-0485\(2004\)034<1528:LGOSOS>2.0.CO;2](https://doi.org/10.1175/1520-0485(2004)034<1528:LGOSOS>2.0.CO;2)
- Yeager, S. G., & Large, W. G. (2007). Observational evidence of winter spice injection. *Journal of Physical Oceanography*, 37(12), 2895–2919. <https://doi.org/10.1175/2007JPO3629.1>
- Zeller, M., McGregor, S., & Spence, P. (2019). Hemispheric asymmetry of the Pacific shallow meridional overturning circulation. *Journal of Geophysical Research: Oceans*, 124, 5765–5786. <https://doi.org/10.1029/2018JC014840> check doi
- Zeller, M., McGregor, S., vanSebille, E., Capotondi, A., & Spence, P. (2021). Subtropical-tropical pathways of spiciness anomalies and their impact on equatorial Pacific temperature. *Climate Dynamics*, 56(3–4), 1131–1144. <https://doi.org/10.1007/s00382-020-05524-8>